

REPORT DOCUMENTATION PAGE			Form Approved OMB No. 0704-0188		
Public reporting burden for this collection of information is estimated to average 1 hour per response, including the time for reviewing instructions, searching existing data sources, gathering and maintaining the data needed, and completing and reviewing the collection of information. Send comments regarding this burden estimate or any other aspect of this collection of information, including suggestions for reducing the burden, to Department of Defense, Washington Headquarters Services, Directorate for Information Operations and Reports (0704-0188), 1215 Jefferson Davis Highway, Suite 1204, Arlington, VA 22202-4302. Respondents should be aware that notwithstanding any other provision of law, no person shall be subject to any penalty for failing to comply with a collection of information if it does not display a currently valid OMB control number. PLEASE DO NOT RETURN YOUR FORM TO THE ABOVE ADDRESS.					
1. REPORT DATE (DD-MM-YYYY) 09-04-2010		2. REPORT TYPE Final Report		3. DATES COVERED (From - To) 9 March 2009 - 09-Mar-10	
4. TITLE AND SUBTITLE Fluid-Structure Interaction of Oscillating Low Aspect Ratio Wings at Low Reynolds Numbers			5a. CONTRACT NUMBER FA8655-09-1-3007		
			5b. GRANT NUMBER		
			5c. PROGRAM ELEMENT NUMBER		
6. AUTHOR(S) Dr. Zhijin Wang			5d. PROJECT NUMBER		
			5d. TASK NUMBER		
			5e. WORK UNIT NUMBER		
7. PERFORMING ORGANIZATION NAME(S) AND ADDRESS(ES) University of Bath Claverton Down Bath BA2 7AY United Kingdom			8. PERFORMING ORGANIZATION REPORT NUMBER N/A		
9. SPONSORING/MONITORING AGENCY NAME(S) AND ADDRESS(ES) EOARD Unit 4515 BOX 14 APO AE 09421			10. SPONSOR/MONITOR'S ACRONYM(S)		
			11. SPONSOR/MONITOR'S REPORT NUMBER(S) Grant 09-3007		
12. DISTRIBUTION/AVAILABILITY STATEMENT Approved for public release; distribution is unlimited.					
13. SUPPLEMENTARY NOTES					
14. ABSTRACT Detailed force measurements on a plunging rectangular wing with semi aspect ratio of 2, at low Reynolds numbers of 10,000-30,000 have been conducted in a water tunnel at various non-dimensional frequencies and amplitudes, alongside particle image velocimetry (PIV) measurements of the flow at the midspan plane and hot film measurements in the wake. The presence of multiple peaks in lift has been identified for this three-dimensional wing, thought to be related to the natural shedding frequency of the stationary wing. Wing/vortex and vortex/vortex interactions have been identified which may also contribute to the selection of optimal frequencies. Lift enhancement is observed to become more notable with increasing amplitude, coupled with a slight shift in the peak frequencies, to lower Strouhal numbers, with 3 increasing angle of attack. Despite the highly three-dimensional nature of the flow, lift enhancements up to 180% are possible. The unsteady aerodynamics of low aspect ratio membrane wings (rectangular wing and delta wing) has been investigated in a Reynolds number range of 24,000 – 59,000. Membrane deformations were measured by using a Digital Image Correlation (DIC) system. Force measurements were conducted for membrane wings and compared with those of rigid wings of similar geometries. The comparison indicates that the effect of flexibility benefits the rectangular wing more than the delta wing by increasing the maximum normal force as well as the slope by a larger amount. Oscillations of the membrane, mode shapes, and the corresponding vibration frequencies were investigated. The combination of tip vortices and leading-edge vortex shedding results in a mixture of streamwise and spanwise vibrational modes. The Strouhal numbers of membrane vibration frequencies are on the order of unity, and have similar range to those of two-dimensional airfoils. The results suggest possible coupling with wake instabilities. The Particle Image Velocimetry (PIV) measurements indicate stronger vortices for membrane wings, which contribute significantly to the total lift. The experimental data obtained in the past 6 months are being used for comparisons with the computational simulations carried out by AFRL.					
15. SUBJECT TERMS EOARD, Experimental, Aerodynamics, Micro Air Vehicle					
16. SECURITY CLASSIFICATION OF:			17. LIMITATION OF ABSTRACT UL	18. NUMBER OF PAGES 19	19a. NAME OF RESPONSIBLE PERSON Surya Surampudi
a. REPORT UNCLAS	b. ABSTRACT UNCLAS	c. THIS PAGE UNCLAS			19b. TELEPHONE NUMBER (Include area code) +44 (0)1895 616021

**FLUID-STRUCTURE INTERACTION OF OSCILLATING LOW ASPECT RATIO
WINGS AT LOW REYNOLDS NUMBERS**

Contract No: FA8655-09-1-3007

Final Report for Months 7-12

submitted to

Dr. Surya Surampudi

**European Office of Aerospace Research & Development (EOARD)
223/231 Old Marylebone Road
NW1 5TH London, UK**

by

**Dr. Zhijin Wang
Department of Mechanical Engineering
University of Bath
Bath, BA2 7AY
United Kingdom**

March 2010

CONTENTS

1. SUMMARY

2. EXPERIMENTAL APPARATUS AND METHODS

2.1 Plunging Rigid Low Aspect Ratio Wings

2.2 Low Aspect Ratio Membrane Wings

3. MAIN FINDINGS

3.1 Plunging Rigid Low Aspect Ratio Rectangular Rigid Wing

3.1.1 Effect of oscillation frequency

3.1.2 Effect of amplitude

3.2 Unsteady Aerodynamics of Low Aspect Ratio Membrane Wings

4. REFERENCES

1. SUMMARY

In months 7-12, detailed force measurements on a plunging rectangular wing with semi aspect ratio of 2, at low Reynolds numbers of 1×10^4 - 3×10^4 have been conducted in a water tunnel at various non-dimensional frequencies and amplitudes, alongside particle image velocimetry (PIV) measurements of the flow at the midspan plane and hotfilm measurements in the wake. The presence of multiple peaks in lift has been identified for this three-dimensional wing, thought to be related to the natural shedding frequency of the stationary wing. Wing/vortex and vortex/vortex interactions have been identified which may also contribute to the selection of optimal frequencies. Lift enhancement is observed to become more notable with increasing amplitude, coupled with a slight shift in the peak frequencies, to lower Strouhal numbers, with

increasing angle of attack. Despite the highly three-dimensional nature of the flow, lift enhancements up to 180% are possible.

The unsteady aerodynamics of low aspect ratio membrane wings (rectangular wing and delta wing) has been investigated in a Reynolds number range of 2.4×10^4 - 5.9×10^4 . Membrane deformations were measured by using a Digital Image Correlation (DIC) system. Force measurements were conducted for membrane wings and compared with those of rigid wings of similar geometries. The comparison indicates that the effect of flexibility benefits the rectangular wing more than the delta wing by increasing the maximum normal force as well as the slope by a larger amount. Oscillations of the membrane, mode shapes, and the corresponding vibration frequencies were investigated. The combination of tip vortices and leading-edge vortex shedding results in a mixture of streamwise and spanwise vibrational modes. The Strouhal numbers of membrane vibration frequencies are on the order of unity, and have similar range to those of two-dimensional airfoils. The results suggest possible coupling with wake instabilities. The Particle Image Velocimetry (PIV) measurements indicate stronger vortices for membrane wings, which contribute significantly to the total lift. The experimental data obtained in the past 6 months are being used for comparisons with the computational simulations carried out by Dr. Visbal's group.

2. EXPERIMENTAL APPARATUS AND METHODS

2.1 Plunging Rigid Low Aspect Ratio Wings

Experiments were carried out in a free-surface closed-loop water tunnel (Eidetics[®] Model 1520) at the University of Bath. The forced plunging motion of a rectangular wing (semi aspect ratio $sAR=2$) with NACA0012 cross-section was provided by a 'shaker mechanism', consisting of an AC 0.37kW Motovario three-phase motor, using a 5:1 gearbox reduction and a basic rotary

to linear mechanism. An illustration of the rig is provided in Figure 1. Flow measurements were obtained using a Digital Particle Image Velocimetry (DPIV) system. The TSI Inc. 2D-PIV system comprises of a dual ND:YAG 120 mJ pulsed laser, and was used to illuminate a streamwise plane. The flow was seeded with 8-12 μm hollow glass particles and the illuminated plane was then captured by a 2MP Powerview Plus 12bit CCD camera. A rotary encoder was used to send a pulse 360 times a second each with a constant time interval. The combination of an trigger system, to isolate a desired pulse from the rotary encoder and the LaserPulse synchroniser, was used to fire the laser at the required point in the cycle. Both phase-averaged and time-averaged measurements were conducted. Captured images were then processed using a commercially available software, TSI Insight 3G, to produce a series of velocity vectors. Force measurements were conducted using a two component binocular load cell. An AD/DA converter converts the signals before being sent to the data acquisition card.

2.2 Low Aspect Ratio Membrane Wings

The experiments were carried out in a low-speed, closed-loop open-jet wind tunnel with a circular working section of 760 mm in diameter, located at the Department of Mechanical Engineering of University of Bath. After discussions with AFRL collaborators (Miguel Visbal), two wings were tested, a rectangular wing with aspect ratio of $AR = 2$ (a chord length of $c = 68.8$ mm) and a delta wing with sweep angle of $\Lambda = 50^\circ$ (a chord length of $c = 82.8$ mm). The dimensions are shown in Figures 2a and 2b. Each wing was composed of a rigid frame and an attached membrane. The wing was attached to a shaft through a strain gauge force balance for making direct force measurements in the normal directions. For the purpose of comparison, force measurements were also conducted on rigid wings. The shaft was driven by a computer controlled step-motor for changing the wing incidences. A high frame rate Digital Image

Correlation (DIC) system, which employs two pre-calibrated CCD cameras, was used to measure the time-accurate membrane displacements. The DIC system employs a mathematical correlation method to measure deformation on an object's surface [1-3]. Experiments were conducted over a range of angle of attack and various Reynolds numbers. Quantitative flow measurements were undertaken using Digital Particle Image Velocimetry (DPIV). The laser sheet was placed parallel to the freestream flow at the mid-span location for the measurements in a streamwise plane as shown in Figure 3a, and perpendicular to the freestream very close to the trailing edge (at 2 mm distance) for the cross-flow measurements as shown in Figure 3b. The commercial software TSI Insight v6.0 and a fast Fourier transform (FFT) cross-correlation algorithm were used to analyze the captured images.

3. MAIN FINDINGS

3.1 Plunging Rigid Low Aspect Ratio Rectangular Rigid Wing

Figure 4 presents the time-averaged lift and drag of the wing oscillating at an amplitude of $h=0.025$ and an incidence of $\alpha=20^\circ$ and indicated Reynolds numbers. A substantial increase in lift is recorded with dominant peaks occurring at $St_c \approx 0.45-0.5$ and $St_c \approx 0.9$. The corresponding lift enhancements are 67% and 75%, respectively, over the stationary case, at $Re=1 \times 10^4$. Increasing the frequency beyond the second peak, results in a plateau being reached, albeit with underlying attenuated undulations. Within a range of $0 \leq St_c \leq 1.2$ the effect of varying the operating Reynolds number between $Re=1 \times 10^4$ and $Re=3 \times 10^4$ has little effect, suggesting that the phenomenon is aerodynamic and not related to any structural resonance or setup-related issues. Although not primarily the motivation for the current study, drag measurements have also been presented, given that there exists considerable interest in the propulsion of oscillating

wings. A peak in drag occurs simultaneously with the initial peak in lift, followed by a gradual reduction with increased frequency, even so, no thrust is produced within the frequency range tested.

The phase-averaged vorticity and velocity magnitude, at the midspan plane, are presented in Figure 5a and Figure 5b, respectively. Figure 5 illustrates the presence of multiple vortices appearing on the suction surface of the wing, the number of which depends on the frequency of the oscillation. Multiple distinct LEVs have been observed in two-dimensional flows [4,5], and evidently still present to at least one chord length outboard of the root of this low aspect ratio wing. At the location of the initial peak in lift, $St_c=0.45$, one can observe the size and location of the generated vortex (LEV_1). Interestingly, at this frequency, a single vortex is observed over the wing, in comparison to the two visible leading-edge vortices over the wing at the second peak in lift ($St_c=0.9$). At subsequent multiples of $St_c=0.9$, an additional leading edge vortex appears, given that the increased forcing frequency reduces, by a similar factor, the distance travelled per cycle. This seems to suggest that these optimal frequencies are selected based on the number of vortices captured by the wing. A coupling between the wake instabilities and vortex/wing interactions may therefore determine these optimal frequencies for lift.

3.1.1 Effect of oscillation frequency

A previous study [6] on the aerodynamic performance of an oscillating two-dimensional NACA0012 profile, elicited the existence of several frequencies at which the time-averaged lift is locally maximised. The forcing frequencies corresponding to such peaks were suggested as being sub-harmonic, fundamental and harmonics of the natural vortex shedding frequency in the wake of the stationary wing at $\alpha=15^\circ$. Figure 6 presents a comparison of the time-averaged lift performance of the two-dimensional airfoil, to the current finite wing of $sAR=2$, in which both

wings are subject to an oscillating amplitude of $h=0.15$, set to $\alpha=20^\circ$, the latter representative of a post-stall condition. Evidently, optimal frequencies exist for the finite wing, roughly adhering to those of the airfoil. A drop of 38-40%, in relation to the local maxima in lift is encountered. As the aspect ratio is reduced, an increasingly noteworthy interaction between wing tip vortices and leading edge vortices occurs [7]. If we consider these imparted peaks to be most effective in two-dimensional flows, added unsteadiness from the aforementioned interaction and thus reduction of assimilative two-dimensional flow neighbouring the midspan, with reduced aspect ratio, will diminish the effectiveness of the generated vortices, resulting in a less distinguishable peak. This is evident from the comparison made in Figure 6, through the apparent attenuation and graduality of the peaks of the low aspect ratio wing.

It was suggested that a natural vortex shedding frequency of $St_c=0.83$, for the airfoil case at $\alpha=15^\circ$ [6], and its sub-harmonic and first-harmonic correspond to the optimal frequencies in lift. Hot-film measurements were performed to investigate wake instabilities for the current wing. A typical signal for the presented case of $\alpha=20^\circ$ and $Re=1 \times 10^4$ is shown in Figure 7. The quasi-periodic nature of the flow at the midspan, is akin to the supercritical mode observed by Huang and Lin [8] and adequate enough to produce a distinct spectral peak, presented in Figure 8. The measured frequencies at three different angles attack are presented in Figure 9 as hollow triangular symbols. A comparison has also been made within Figure 9 with the vortex shedding frequencies reported by Huang and Lin [8] using the same NACA0012 profile at $Re=1.1 \times 10^4$, albeit with a larger semi aspect ratio of 5. The results reveal a surprisingly remarkable fit, despite the lower aspect ratio of the current wing. Superimposed within the same graph are the locations of the first and second time-averaged lift peaks for the three angles of attack that have been tested in the present study. Figure 9 shows that the first peak for $\alpha=20^\circ$, is very close to the

natural vortex shedding frequency in the wake. However, for $\alpha=10^\circ$, the data seem to suggest that the first peak could be the sub-harmonic of the natural vortex shedding frequency. The interpretation is even more difficult for $\alpha=15^\circ$, for which the first peak corresponds to the sub harmonic in the two-dimensional airfoil case [6]. It is apparent that the peaks in lift are in the same order as the frequencies of the wake instabilities of the stationary wing. However, the first peak remains remarkably unchanged for all three incidences, while the fundamental frequency of the wake instability varies.

3.1.2 Effect of amplitude

Figure 10 presents lift and drag measurements for the wing oscillating with an amplitude of $h=0.15$ for all Re cases. This is presented with the measurements for $h=0.025$ operating at $Re=1\times 10^4$. There is an immediate benefit to operating at this higher amplitude. Quantitatively, what was originally observed to be a 67% increase in lift at $St_c=0.45$ for $h=0.025$, transforms to an increase of 126% over the static case for $h=0.15$. Moreover, the change in amplitude has, within experimental uncertainty, unaffected the required forcing frequency of the local peak in lift. Again, little difference can be inferred between the Reynolds numbers tested. The switch from drag to thrust occurs within the operational range of Strouhal numbers, at $St_c\approx 1.1-1.25$.

Figure 11 shows the phase-averaged vorticity contour plots for varying St_c , at various locations in the cycle. Analogously to the lower amplitude case, as the frequency is increased, the vortices form closer to the surface with greater coherency. Notice the LEV formed at $St_c=0.2$ compared to $St_c=0.45$. The increased frequency evokes a relatively lower convection distance within the cycle, allowing the vortex to remain close to the upper surface, through to the bottom of the cycle. The delayed shedding of the vortex would imply a more effective form of lift production, resulting in the monotonic rise in lift up to a Strouhal number of $St_c=0.45$. Further

increasing the forcing frequency, encourages this delay, eventually preventing the leading edge vortex from passing the trailing edge vortex formed in the following cycle. Once again, in a similar fashion to $h=0.025$, two LEVs are present on the upper surface, at the bottom of the oscillation, for $St_c=0.9$ (Figure 11a). Although the LEV, from the preceding cycle, is located further away from the upper surface of the wing, than that of $h=0.025$, the streamwise convection distance is very similar. A further increase in frequency has the effect of causing a destructive interaction between the wing and LEV, similar to that of the two-dimensional airfoil. This is clearly observed for $St_c=2.0$, for which the LEV is absent at the top of the oscillation ($t/T=1.0$). This in effect precludes any further formation of multiple vortices on the upper surface.

3.2 Unsteady Aerodynamics of Low Aspect Ratio Membrane Wings

Figure 12 presents the variation of the maximum magnitudes of z-displacement as a function of angle of attack of the rectangular wing for different freestream velocities. For the lowest freestream velocity $U_\infty = 5$ m/s, the maximum displacement increases gradually up to about $\alpha = 20^\circ$, then stays roughly constant. The membrane generates a larger magnitude of the maximum camber as the freestream velocity is increased. Notably, there is also camber at zero angle of attack particularly at $U_\infty = 10$ m/s. The variation of the maximum magnitudes of the normalized displacement of the delta wing as a function of angle of attack is shown in Figure 13 for different freestream velocities. Generally, the delta wing exhibits similar trend of the variations in displacements to those of the rectangular wing, but with smaller magnitude. For $U_\infty = 5$ m/s and at small incidences, the slope is relatively steep which means that the membrane cambering is more sensitive to the change in angles of attack within this range. For this freestream velocity, the maximum displacement increases gradually up to about $\alpha = 21^\circ$. Once again the membrane shows a larger magnitude of the maximum displacement as the freestream velocity is increased.

However, the rate of the increase of the maximum displacement z_{\max}/c with angle of attack α is smaller for the higher freestream velocities.

The variation of the time-averaged normal force coefficient is shown as a function of angle of attack in Figure 14 for the membrane and rigid rectangular wings at different freestream velocities. Even though the displacement slopes (Figure 12) are not linear, the normal force slope is nearly linear until the stall. The flexible membrane wings have higher slopes than the rigid wing, and the stall angles are only slightly affected. These favorable larger slopes are not unexpected as the induced wing camber increases with increasing angle of attack. However, the corresponding increase in the camber alone does not explain the significant increase in the force slope. In addition, it is observed that the membrane wings start to generate the lift at $\alpha = 0^\circ$. This is consistent with the wing's maximum displacement (Figure 12) which shows a small camber at zero angle of attack. At the highest freestream velocity, $U_\infty = 10$ m/s, the membrane wing reaches the highest maximum normal force coefficient $C_{n,\max}$ of approximately 1.26, which is about 1.5 times of that of the rigid wing. Similar to the rectangular wing, the flexible delta wing exhibits a larger time-averaged normal force coefficient than the rigid delta wing as shown in Figure 15. At the highest freestream velocity, $U_\infty = 10$ m/s, the membrane wing reaches the highest $C_{n,\max}$ of 1.16, which is approximately 1.2 times that of the rigid wing.

Figure 16 shows the frequency spectra computed from the z-displacement of the membrane sampled at the point of maximum standard deviation at $U_\infty = 10$ m/s. For small incidences, the dominant normalized frequencies (Strouhal numbers $Sr = fc/U_\infty$) are rather difficult to identify, suggesting that the magnitudes of vibration are very small. However, starting around $\alpha = 7^\circ - 9^\circ$, the dominant normalized frequencies fall in a well-defined band, and on the order of unity. Within certain ranges of angles of attack, there seems to be higher modes. Of course, the change

in the dominant frequencies is related to the change in the mode shapes. At high incidences, where the second mode is always observed for all the velocities tested, the Strouhal numbers are in a similar range with those of the two-dimensional membrane airfoils [9]. For two-dimensional membrane airfoils, the oscillation in this range suggests the coupling with the vortex shedding in the wake. Therefore, the present results suggest a possible coupling of membrane oscillation for the rectangular wing with the wake instabilities.

Figure 17 shows the comparison of the magnitude of the time-averaged velocity field superimposed on the streamline pattern for the rectangular wings at selected angles of attack. The data were taken for the rigid wing at $U_\infty = 5$ m/s, and the membrane wing at $U_\infty = 5$ m/s and 10 m/s. Starting with small incidence $\alpha = 5^\circ$, the flow remains attached for all wings. At higher angle of attack $\alpha = 10^\circ$, the flow on the rigid wing becomes separated. For $\alpha = 16^\circ$, the shear layer moves away from the surface for the rigid wing, while the flow on the membrane wing is separated but the shear layer remains close to the surface. It is also seen that at this angle of attack, with increasing freestream velocity to $U_\infty = 10$ m/s, the shear layer for the membrane wing is getting closer to the wing surface while the camber of the wing increases. The effect of increasing freestream velocity is consistent with the previous work for two-dimensional membrane airfoils [9,10]. The separated shear layer moves further away from the surface with increasing angle of attack to $\alpha = 23^\circ$ for all wings. Again, the separation region is largest for the rigid wing, and smallest for the membrane wing with $U_\infty = 10$ m/s. For the latter, the closed streamline pattern (recirculation region) is seen over the wing surface, while it is located further downstream for the lower freestream velocity, and even further away from the trailing edge for the rigid wing.

Figure 18 shows the magnitude of the time-averaged velocity in a cross-flow plane near the trailing edge for the rectangular rigid and membrane wings. The cross-flow velocity is seen to increase with increasing flexibility. This suggests stronger tip vortices with increasing camber. The variation of normalized circulation of tip vortices (not shown), calculated from the area integral of vorticity distributions in the cross-flow plane based on the PIV measurements, suggested that membrane wing has a larger magnitude of the circulation than the rigid wing for both freestream velocities. Since the tip vortices (and vortex lift) contribute significantly to the total lift, this may be an additional mechanism for the increased lift with increasing membrane deformation. Whereas the normalized circulation of the rigid wing remains virtually unchanged with increasing freestream velocity (Reynolds number), the normalized circulation increases for the membrane wing.

4. REFERENCES

- [1] Chu, T. C., Ranson, W. F., Sutton, M. A., and Peters, W. H., "Applications of Digital-Image-Correlation Techniques to Experimental Mechanics," *Experimental Mechanics*, Vol. 25, No. 3, 1985, pp. 232-244.
- [2] Bruck, H. A., McNeill, S. R., Sutton, M. A., and Peters, W. H., "Digital Image Correlation using Newton-Raphson Method of Partial Differential Correction," *Experimental Mechanics*, Vol. 29, No. 3, 1989, pp. 261-267.
- [3] Peters, W. H., and Ranson, W. F., "Digital Imaging Techniques in Experimental Stress Analysis," *Optical Engineering*, Vol. 21, 1982, pp. 427-431.
- [4] Visbal, M.R. "High-Fidelity Simulation of Transitional Flows Past a Plunging Airfoil", *47th AIAA Aerospace Sciences Meeting*, Orlando, Florida, 2009, AIAA Paper 2009-391.

- [5] Cleaver, D.J., Wang, Z.J. and Gursul, I. . "Delay of Stall by Small Amplitude Airfoil Oscillation at Low Reynolds Numbers", *47th AIAA Aerospace Sciences Meeting*, Orlando, Florida, 2009, AIAA Paper 2009-392.
- [6] Cleaver, D.J., Wang, Z.J. and Gursul, I. . "Lift Enhancement on Oscillating Airfoils", *39th AIAA Fluid Dynamics Conference*, San Antonio, Texas, 2009, AIAA Paper 2009-4028.
- [7] Dong, H., Mittal, R. and Najjar, F.M. "Wake Topology and Hydrodynamic Performance of Low-Aspect-Ratio Flapping Foils", *Journal of Fluid Mechanics*, Vol. 566, 2006, pp. 309-343.
- [8] Huang, R.F. and Lin, C.L. "Vortex Shedding and Shear-Layer Instability of Wing at Low-Reynolds Numbers", *AIAA Journal*, Vol. 33, No. 8, 1995, pp. 1398-1403.
- [9] Rojratsirikul, P., Wang, Z., and Gursul, I., "Effects of Pre-Strain and Excess Length on Unsteady Fluid-Structure Interactions of Membrane Airfoils," *47th AIAA Aerospace Sciences Meeting and Exhibit*, 5-8 Jan. 2009, Orlando, Florida, AIAA 2009-578, pp. 1-20.
- [10] Rojratsirikul, P., Wang, Z., and Gursul, I., "Unsteady Fluid–Structure Interactions of Membrane Airfoils at Low Reynolds Numbers," *Experiments in Fluids*, Vol. 46, No. 5, 2009, pp. 859-872.

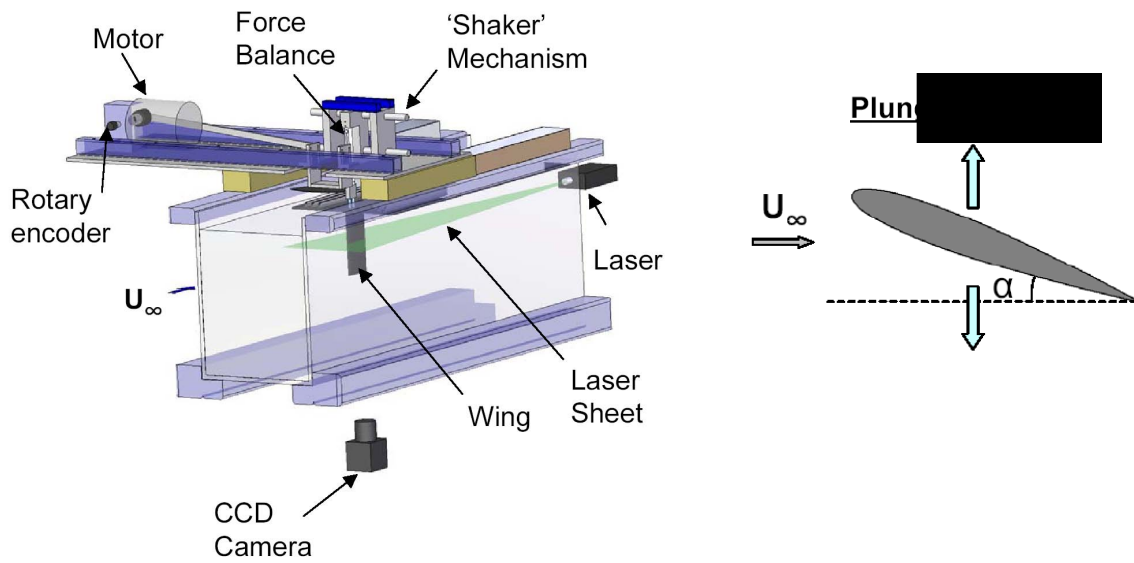


Figure 1. An illustration of the water tunnel experimental setup and apparatus

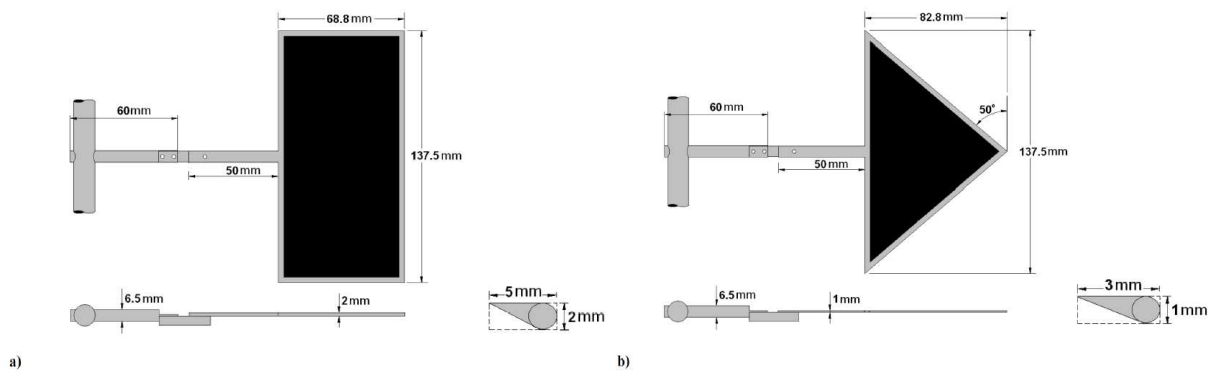


Figure 2. Schematic of the wings with cross-section of the rigid frame; a) Rectangular wing; b) Delta wing.

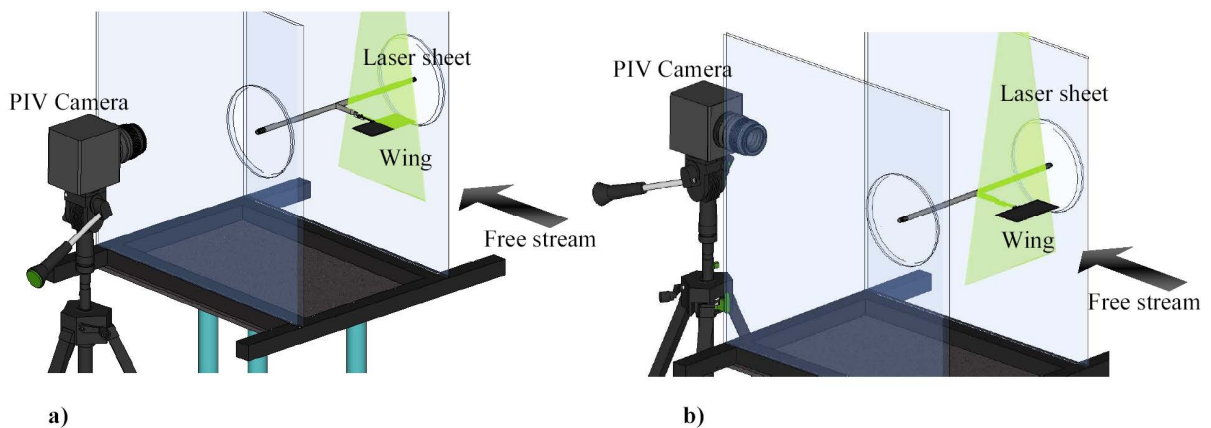


Figure 3. Schematic of PIV measurements for: a) streamwise plane at a mid-span and b) crossflow plane near trailing-edge.

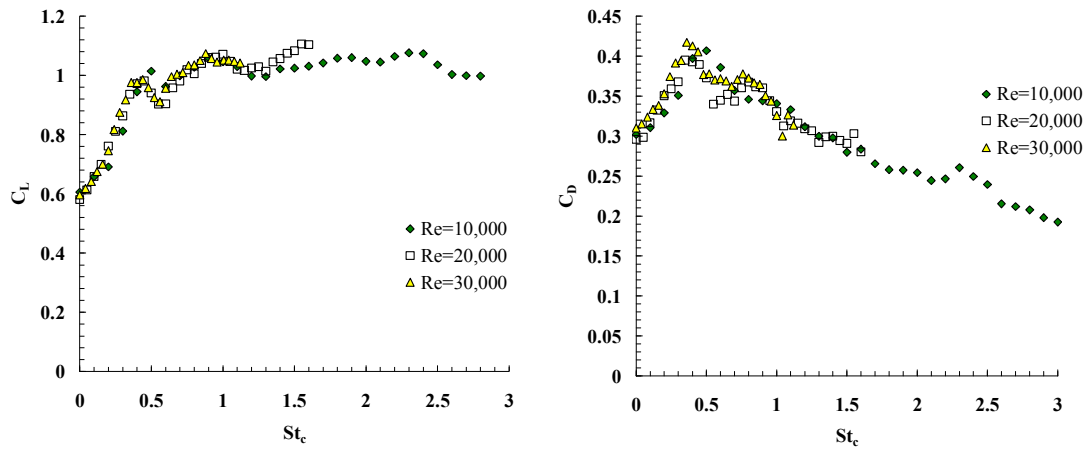


Figure 4. Time averaged lift (left) and drag (right) measurements for the wing oscillating at $h=0.025$, $\alpha=20^\circ$ and indicated Re.

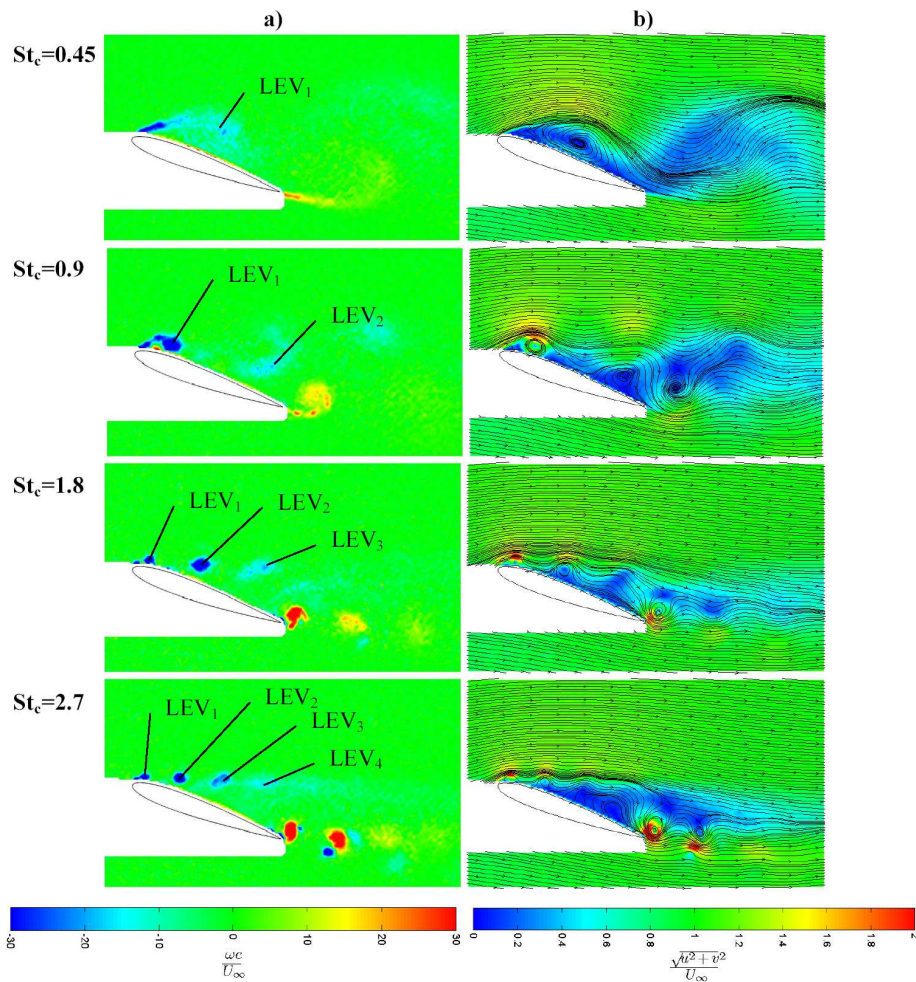


Figure 5. Phase-averaged a) vorticity contours and b) streamlines for $h=0.025$, $Re=1 \times 10^4$ and $\alpha=20^\circ$ at $t/T=0.5$ (bottom of the motion). Each LEV_i represents a vortex formed in a separate cycle.

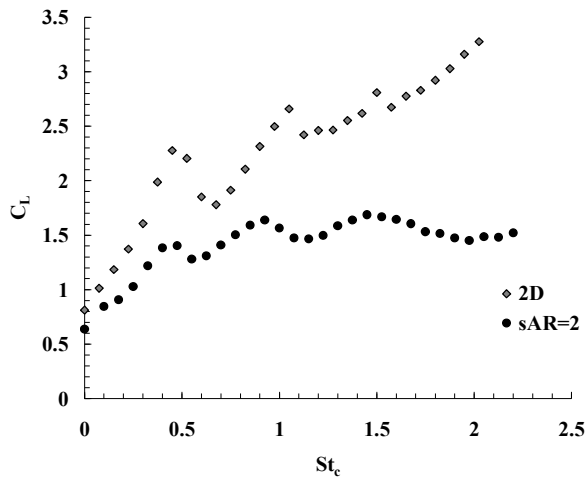


Figure 6. A comparison between the time-averaged lift coefficients of the 2D and sAR=2 NACA0012 wing oscillating at $h=0.15$ and $\alpha=20^\circ$, for $Re=1 \times 10^4$.

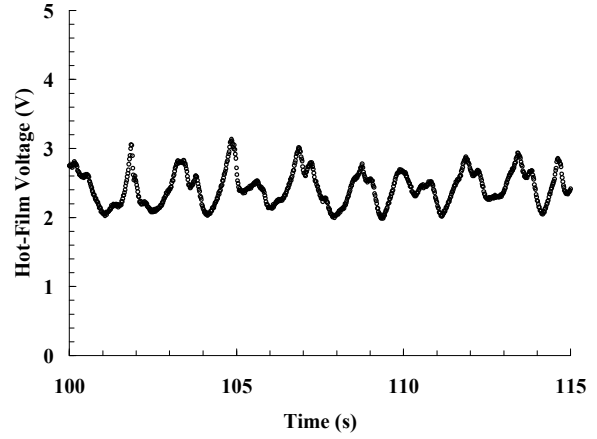


Figure 7. Time-series of the wake velocity for the stationary wing at $\alpha=20^\circ$. $x/c=0.5$, $y/c=-0.2$ and $z/c=1$. The streamwise (x) and cross-stream (y) distance are measured from the trailing edge.

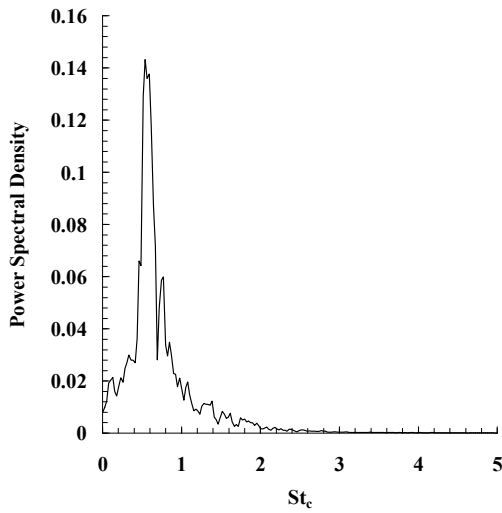


Figure 8. Spectral analysis of the wake velocity for the stationary wing at $\alpha=20^\circ$. $x/c=0.5$, $y/c=-0.2$ and $z/c=1$. The streamwise (x) and cross-stream (y) distance are measured from the trailing edge.

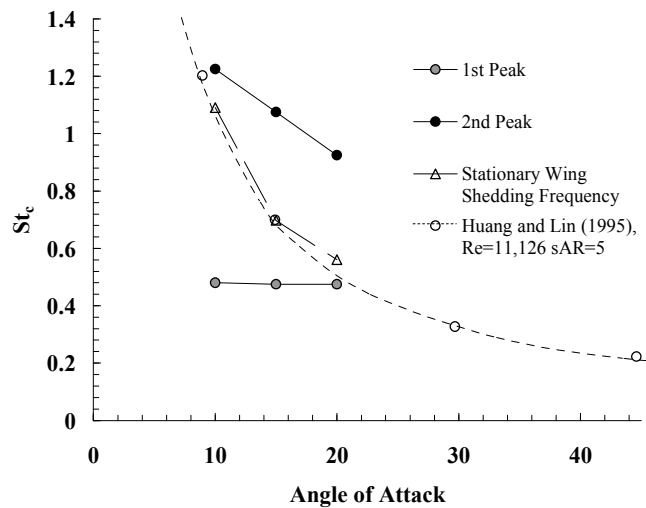


Figure 9. Variation of peaks in lift coefficient for $h=0.15$, $Re=1 \times 10^4$, in relation to the natural vortex shedding frequencies of the stationary wing.

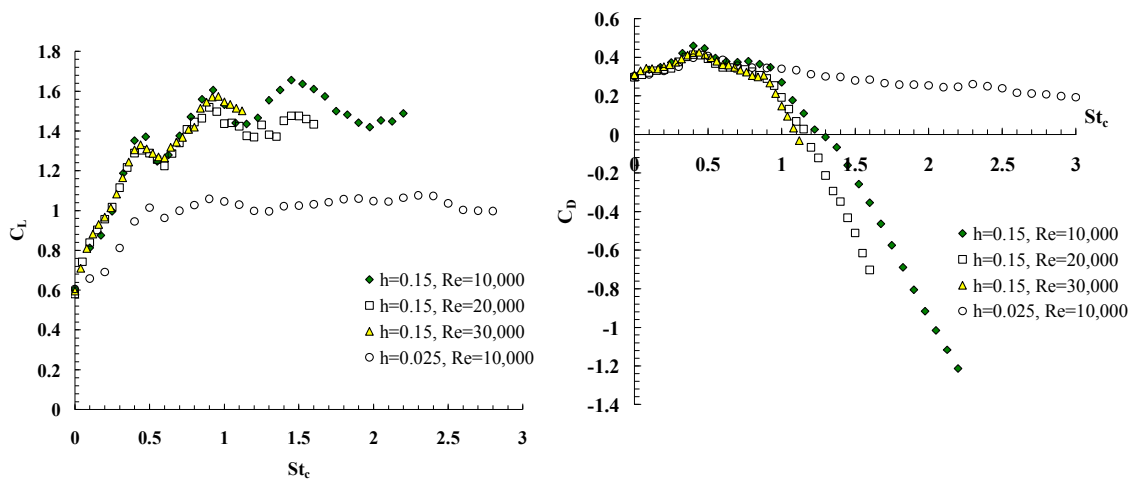


Figure 10. Time-averaged lift (left) and drag (right) measurements for $h=0.15$, $\alpha=20^\circ$ and indicated Re .

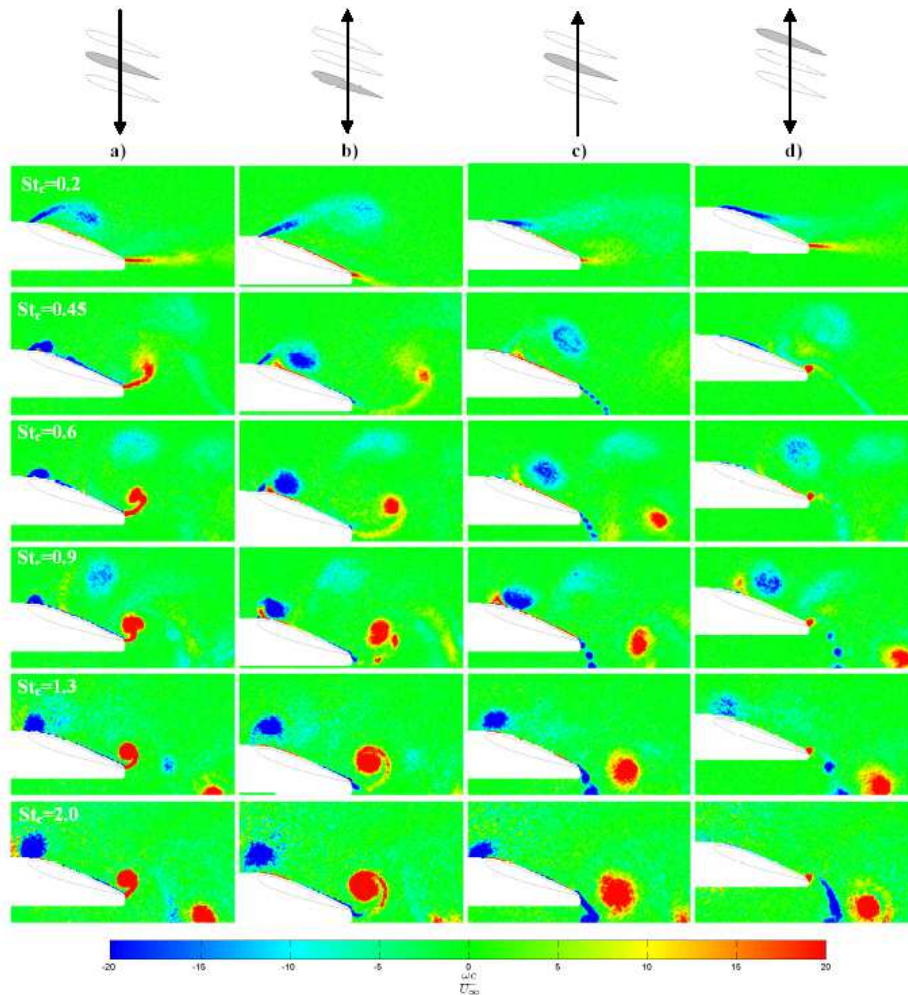


Figure 11. Phase-averaged normalised vorticity plots for $h=0.15$, $\alpha=20^\circ$, $Re=1 \times 10^4$ and stated St_c , at a) $t/T=0.25$, b) $t/T=0.5$, c) $t/T=0.75$, d) $t/T=1.0$.

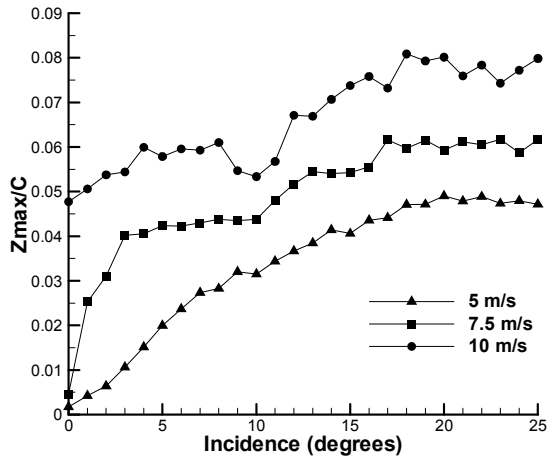


Figure 12. Maximum magnitude of time-averaged displacement as a function of incidence for the rectangular wing.

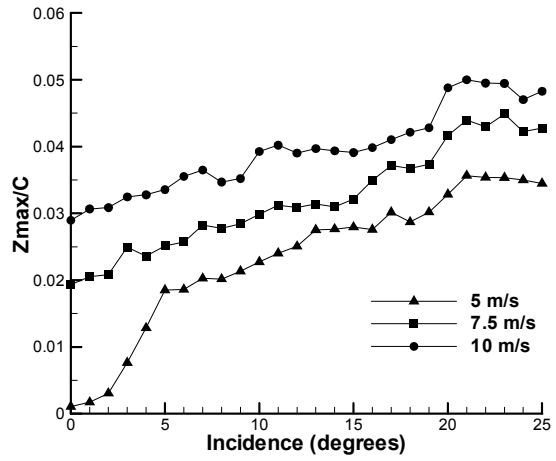


Figure 13. Maximum magnitude of time-averaged displacement as a function of incidence for the delta wing.

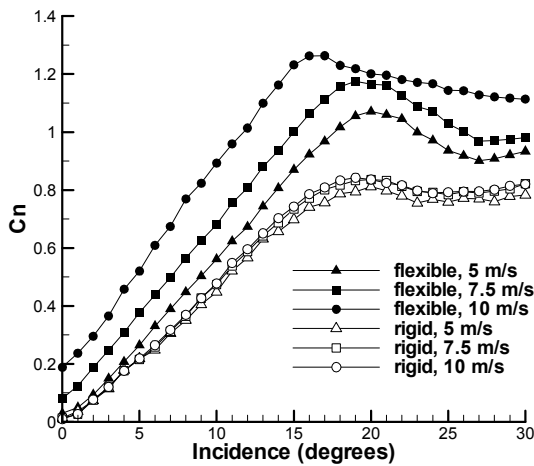


Figure 14. Normal force coefficient as a function of incidence for the flexible and rigid rectangular wings.

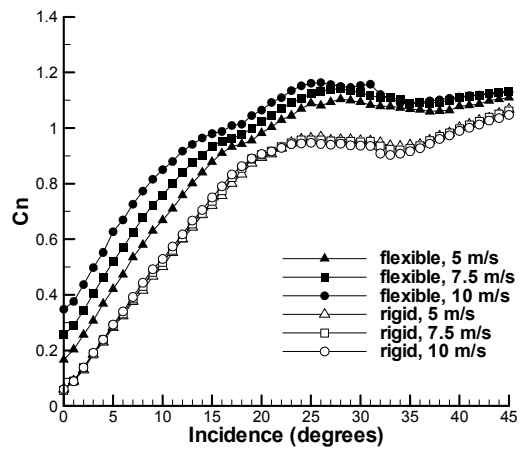


Figure 15. Normal force coefficient as a function of incidence for the flexible and rigid delta wings.

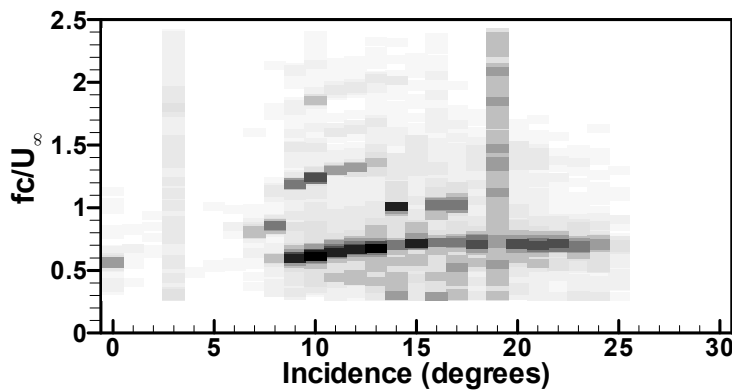


Figure 16. Power spectra of the membrane oscillations as a function of angle of attack for the rectangular wing at $U_\infty = 10$ m/s.

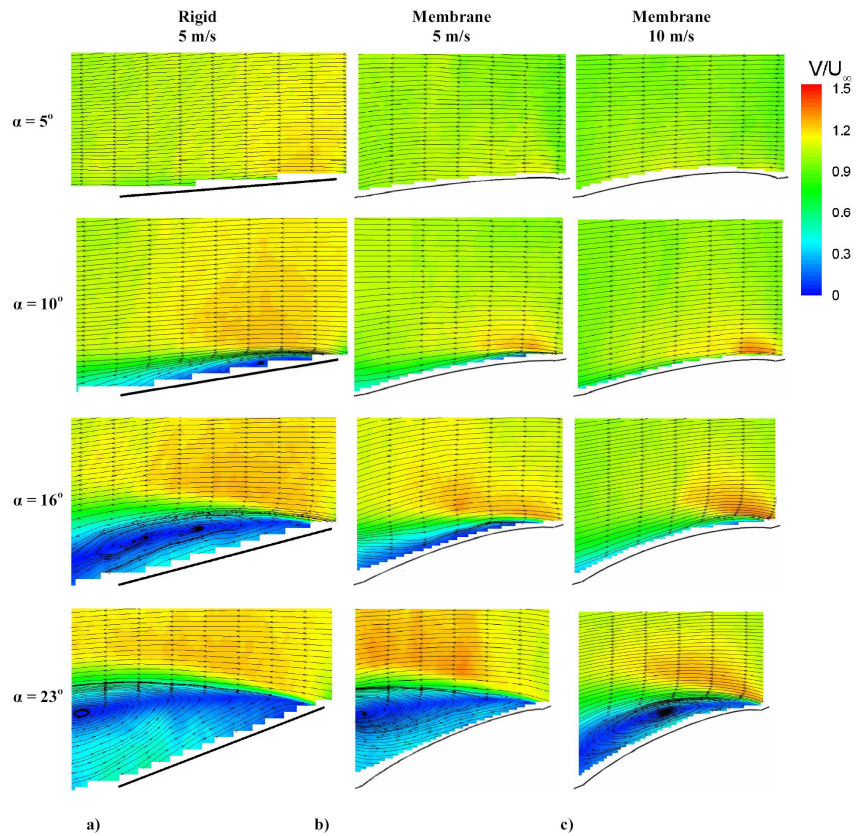


Figure 17. Magnitude of the time-averaged velocity and streamlines in a mid-span plane for the rectangular wings; a) rigid wing $U_\infty = 5$ m/s; b) membrane wing $U_\infty = 5$ m/s; c) membrane wing $U_\infty = 10$ m/s. Flow is from right to left.

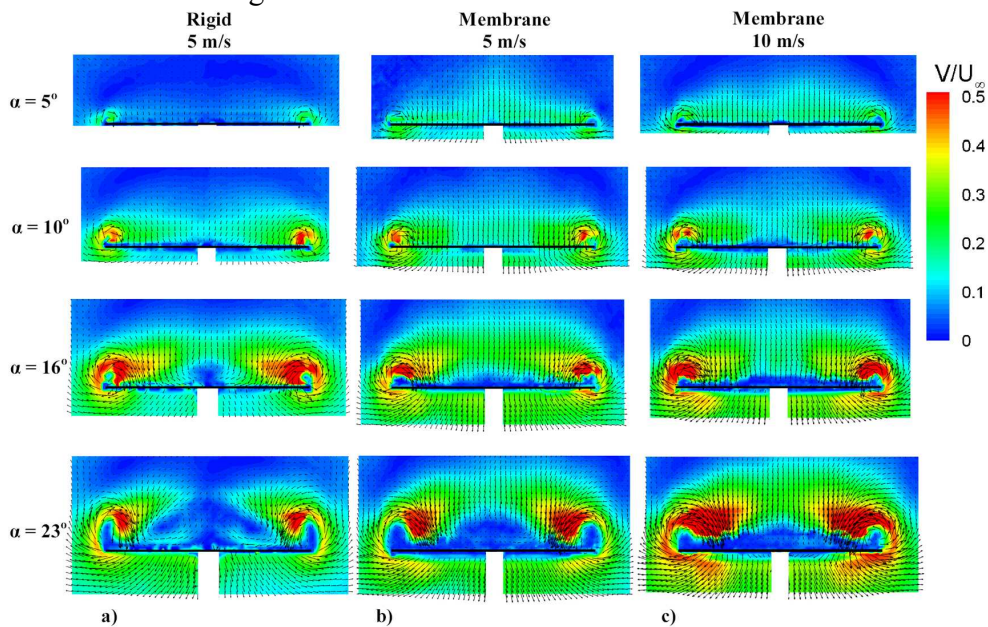


Figure 18. Magnitude of the time-averaged velocity in a crossflow plane near the trailing edge for the rectangular wings; a) rigid wing $U_\infty = 5$ m/s; b) membrane wing $U_\infty = 5$ m/s; c) membrane wing $U_\infty = 10$ m/s.